Evolution of Grounding Failure-Insulation Failure of 10 kV Cable Joints: Prerequisites of an Explosion in Enclosed Cable Trench

Yifeng Zhao [1], Gang Liu [1,2], Yaodong Guo [3], Chenglong Huang[1], Zhaoming He[1], Ran Hu[1,3*]

[1] School of Electric Power Engineering, South China University of Technology, Guangzhou, Guangdong, 510640, China
[2] Pazhou Lab, Guangzhou, Guangdong, 510330, China
[3] Shenzhen Power Supply Bureau Co., Ltd, Shenzhen, Guangdong, 518001, China
[*]corresponding. huran@sz.csg.cn.

Abstract: An explosion accident in an enclosed cable trench caused by the discharge of 10 kV three-phase cable joints is discussed. Combined with the disassembly analysis, the fault recording data analysis, and the validation of experiment, the evolution of the cable joint fault is deduced and discussed. The results show that the trigger of the cable joint fault is the creepage discharge at the XLPE-SiR insulation interface. This results in the partial breakdown and the grounding failure of three-phase cable joints. Under the long-term floating potential and current thermal effect, the insulations are gradually ablated and decomposed into a large amount of combustible gas. Finally, the accumulated combustible gas is ignited by the arc caused by a three-phase short circuit at the moment of the reclosing operation. The analytical method and conclusions proposed in this paper can provide suggestions and guidance for the analysis of similar fault accidents in the future.

1. Introduction

The power distribution system is increasingly important due to the increasing number of branches and growing complexity [1-3]. As the ultimate power supply link to the user, the relay protection has played a significant role in preventing problems at one point in the network from spreading and causing disturbances in other parts of the circuit [4]. However, compared with the high-voltage transmission system, the relay protection settings of the power distribution system are relatively loose. It is mainly reflected in the reclosing operation after trip protection, large setting current, and long setting time. Such settings conform to the principle of electricity reliability, but it also becomes the hidden peril of serious faults in the power distribution system. Currently, the fault analysis of distribution networks has received more and more attention. In [5], time characteristics of electric breakdown and arcing in power cables were presented by experimental investigations and calculations of arcing at ground faults in distribution networks up to 35 kV. Literature [6] presented the results of a complex analysis of amplitude, velocity and time parameters for currents and voltages at arcing ground fault in the 6-kV network. In literature [7], a modified formula for calculating the arc impedance of cable grounding fault in medium voltage cable networks was presented. The results showed that the arc impedance may reduce the fault current and make the relay protection not work correctly.

As the weak point of the power distribution system, the cable joint is prone to serious accidents [8, 9]. Currently, the type of cold-contract silicone rubber (SiR) cable joint is generally adopted. The statistic shows that a large percentage of in-service cable faults occur within the first few years of their service life, which is mostly caused by cable joints [10]. This phenomenon is mainly ascribed to the defects introduced during installation. In [11], artificial defects in cable joints such as protrusion defect, void defect, interface filled with silicone oil, and interface without silicone were designed to explore the discharge behavior, and the corresponding partial discharge characteristics were identified. Y. Z. Arief et al. [12] dealt with partial discharge causing degradation of XLPE cable joint and interfacial phenomena of XLPE/EPR interface due to artificial defects such as metal particles, needle-like void and fiber soaked with water. It is found that phase-resolved partial discharge patterns depend upon the defect type varying with aging time. G. Li et al. [13] established an interface defect model to analyze the effects of typical moisture defect forms and moisture positions on electric field distributions. The result shows that the electric field distortion caused by water trees' defect is the most serious, followed by water film defects and water droplet defects. However, the discharge behavior of actual faulty cable joints is more complicated. In previous studies in engineering failure analysis of the cable joint, Huang et al. [14] analyzed a breakdown fault case of 110 kV combined prefabricated cable joint. It is found that the floating potential caused by grounding failure is responsible for the epoxy insulator breakdown. Liao et al. [15] analyzed a breakdown accident of 220 kV cable joint with large expanding rate under closing overvoltage. It is found that the initiation and development of electric trees occurring in the silicon rubber insulation are associated with the large circumferential stress of the cable joint and overvoltage induced by closing operation. Recently, Hu et al. [16] analyzed a breakdown fault accident of 20 kV cable joint caused by the ablation of the grounded copper mesh. Combined with the circuit simulation model and the finite element method, it is revealed that the transient grounding faults arise from moisture at the internal interface of the cable joint, which may damage the grounding protection line and lead to serious accidents. This provides a vital idea to analyze the distribution network faults from the perspective of protective relaying system.

Since few cable joint failure cases are effectively recorded currently, the dynamic development process of cable joint fault has not been well revealed, medium voltage cable joint in particular. In this paper, an explosion accident caused by various discharge behaviors of distribution network cable joints is taken as an example. Firstly, the operating information of the fault cable line is obtained from the disassembling inspection and the quantitative analysis of fault recording data; Secondly, the verification experiment is implemented to reproduce the evolution of the discharge behaviors in the cable joints. Thirdly, the evolution of the explosion accident is deduced and discussed sufficiently. This research provides references and suggestions for the analysis of similar accidents in the future.

2. Background

2.1. Description of the explosion accident

The explosion accident studied in this paper occurred on a 10-kV pure cable line in Shenzhen city, Guangdong province, China. The partial diagram of the electrical connection of the faulty transmission line is shown in Fig. 1. Feeder automation system with reclosing operation is adopted in this transmission line. In light of the record of relay protection, more than 10 industrial clients powered by the 10-kV feeder of the main transformer in substation A reported that low-voltage trips were operated. After investigation, it was found that the voltage drop of the main transformer was caused by a three-phase short circuit of an unloaded transmission line between Ring-network cabinet B and Circuit breaker cabinet C. Specific trip protection operations in substation A are as follows. At 09:54 am on October 9, 2021, 1st trip protection caused by a two-phase short circuit of B and C phases was activated. Subsequently, 1st recloser was activated, leading to the three-phase short circuit. Finally, 2nd trip protection was activated and the 2nd recloser failed to be activated.

At the scene in Fig. 1, an explosion accident was witnessed in a cable trench. Three cement panels were lifted due to the explosion, one of which was lifted about 3 meters high, and two of which were lifted about 1 meter high. After the accident, it is found that the whole cable trench was

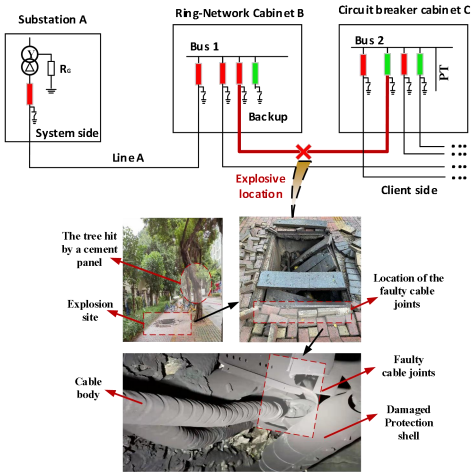

Fig. 1. Electrical connection of the faulty transmission line and the scene of the explosion accident

blackened, and the protection shell of the faulty cable joints has been burned down. According to the field measurement, the cable trench is about 8 meters long, 1.2 meters wide and 0.8 meters deep. Both ends of the cable trench are laid with pipes and the cement panels have no air vents. Therefore, the cable trench becomes an enclosed space. The ambient temperature was 29 ℃ and the air relative humidity was 92% at that time in the cable trench. Additionally, it was measured that the insulation resistance of three-phase lines was 0 Ω.

2.2. Disassembling inspection of the faulty cable joints

The type of fault three-phase cable joints is cold-shrinkable with a configuration of YJV22-3*300 mm2. The cable joints were put into operation on December 30, 2004. For the convenience of the following analysis of disassembling inspection, the single-phase cable joint is divided into high-voltage system, grounding system, and insulation system, as shown in Fig.2. Where the high-voltage system consists of copper conductor of the cable body and crimping pipe of the cable joint; the grounding system consists of copper tape shield of the cable body, and copper mesh and copper braided strip of the cable joint; the

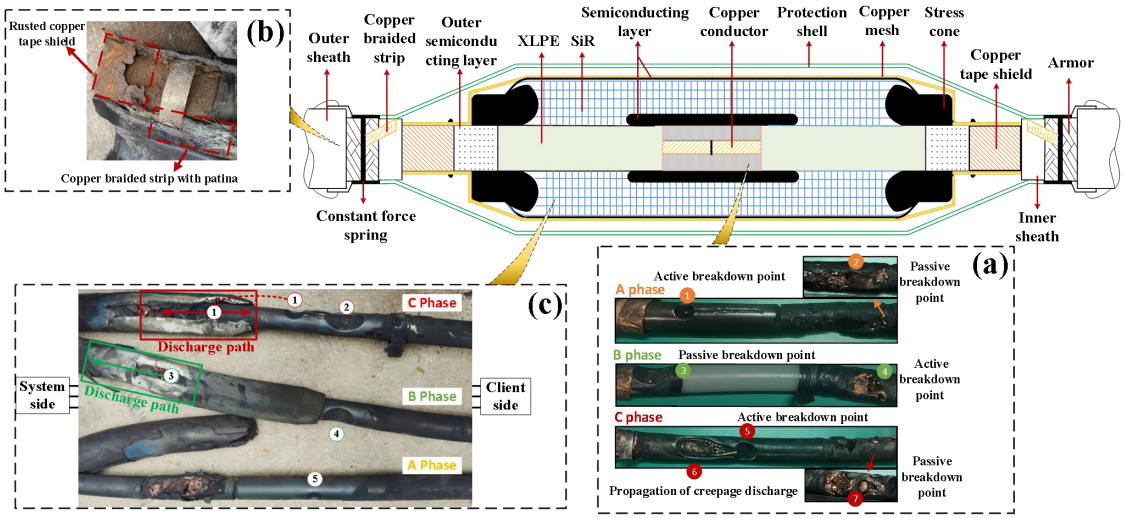

Fig.2. *Damage morphology of the faulty cable joint*
(a) High voltage system, ***(b)*** Grounding system, ***(c)*** Insulation system

insulation system consists of cross-linked polyethylene (XLPE) of the cable body, silicon rubber (SiR) of the cable joint and XLPE-SiR insulation interface.

2.2.1 Disassembly analysis of the high voltage system of the faulty cable joints: Each phase cable joint is disassembled to observe the damage of its high-voltage system, and the details are displayed in Fig.2(a). It is observed that crimping pipes of three-phase cable joints are broken down and the copper conductors are exposed. For B phase cable joint, the protuberant morphology of the copper conductor at position ④ indicates this is an active breakdown point. On the contrary, position ② and position ⑦ of the other two-phase joints show these are passive breakdown points. Additionally, there are obvious active breakdown points at position ① and position ⑤ where they locate at the end of the stress cone. Further, the smooth damage morphology at position ⑥ of C phase is probably ascribed to creepage discharge from position ⑤. Subsequently, the breakdown point at position ③ of B phase appears due to the discharge of position ⑥.

2.2.2 Disassembly analysis of the grounding system of the faulty cable joints: Both the copper tape shield of the cable body, and the copper mesh and the copper braided strip of the cable joint ensure the grounding current flows back to the system side when a grounding fault occurs. If the copper mesh and the copper braided strip of the cable joint were broken, the grounding current through the copper tape shield of the cable body would not be conducted to the system side, and the grounding trip protection would fail to be activated. Figure 2(b) shows the damage morphology of the grounding system of the faulty cable joints. It is inspected that the copper tape shields at both ends of the cable joints are seriously rusted due to water erosion. The residual copper braided strips are covered by patina, and the copper meshes are burnt down. Therefore, the grounding system of the faulty three-phase cable joints has completely failed.

2.2.3 Disassembly analysis of the insulation system of the faulty cable joints: Figure 2(c) shows the damage morphology of the insulation system of the faulty cable joints. For C phase cable joint, it is observed that there is an obvious creepage discharge trace at the XLPE-SiR insulation interface. At the end of the stress cone, there is a distinct breakdown point ①. A large current generated at this point flows to the system side through the copper mesh and copper braided strip. The bidirectional discharge path is shown in Fig. 2(c). The current thermal effect leads to the SiR turning into SiO2 and the partial destruction of the copper mesh. Then, the large current can only flow to the system side through the copper braided strip on the right side of the cable joint. On the one hand, the current carbonizes the outer semiconducting layer of the cable body, leading to the formation of breakdown point ①. On the other hand, the current greatly impacts the copper braided strip and eventually results in its breakage.

For B phase cable joint, there is no creepage discharge trace at the XLPE-SiR insulation interface. However, apparent breakdown point ③ is observed. A large current generated at this point flows to the system side through the copper mesh, which is responsible for the discharge path in Fig. 2(c). Moreover, there is a breakdown point ④ in the cable body.

The damage morphology of A phase cable joint resembles C phase cable joint. There is an obvious creepage discharge trace at the XLPE-SiR insulation interface. In addition, breakdown point ⑤ is found at the end of the stress cone.

3. Quantitative analysis of fault recording data

The transmission line in the distribution network system is electrically connected by low-resistance grounding at both ends. The connection diagram in Fig. 1 can be simplified into the circuit topology diagram in Fig. 3. Where r_{cu}^{A}、r_{cu}^{B} and r_{cu}^{C} are the equivalent resistance of copper tape shield and partial copper mesh, Ω; R_{G1} and R_{G2} are the system neutral grounding resistance, with the value of 16.0 Ω; r_G is the resistance of the earth, Ω. When the transmission line is in a normal-operating state, the branches of r_{cu}^{A}, r_{cu}^{B} and r_{cu}^{C} are regarded as open circuits. However, when the grounding fault of certain phase(s) occurs, the branch(es) is (are) connected between the fault location and the system side. Further, zero-sequence protection may be activated. In addition, Fig. 3 exhibits the 9: 27 am recording data in Substation A before the explosion accident, which well records the dynamic changes of the fault state of the three-phase cable joints.

In Fig.3, it is divided into four fault stages according to the voltage change of three phases. At Stage 1, the voltage of A and B phases is lifted due to the descent in the voltage of C phase. At Stage 2, the voltage of B phase is decreased with C phase. At Stage 3, the voltage of the three phases is declined at the same time, lasting for 158 ms. At this stage, 1st zero-sequence protection trip is activated, and the three-phase voltages become normal. After 370 ms, 1st reclosing operation is triggered, and Stage 4 arrived. Similarly, another three-phase voltage drop lasts for 293 ms and results in the operation of 2nd zero-sequence protection trip. After the subsequent 2nd reclosing operation, the

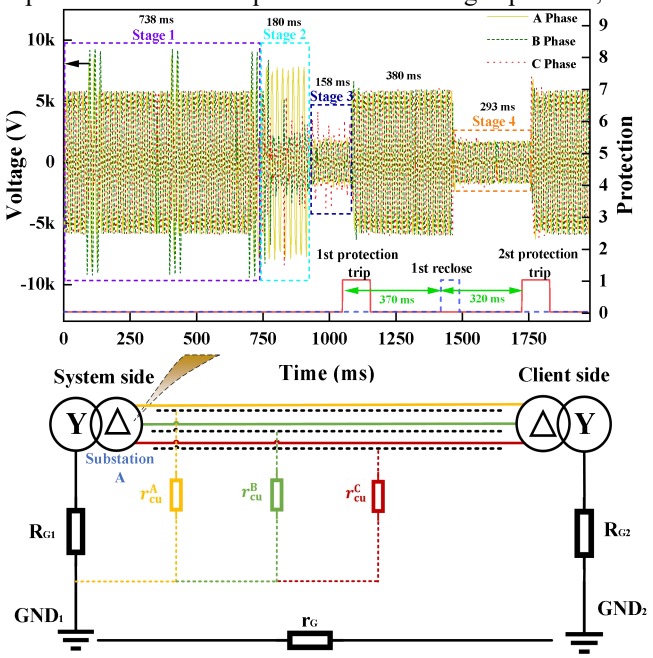

Fig.3 *Circuit topology diagram and the recording data before the explosion accident at 9: 27 am*

protection identifies that the line returns to normal, and the fault recording data is ceased. From the fault recording data, it is deduced that the fault line has gone through the fault state of high resistance grounding fault, low resistance grounding fault, and grounding failure. In the following research, the fault recording data of each stage will be quantitatively analyzed.

3.1. Quantitative analysis at Stage 4

The fault recording data at Stage 4 is exhibited in Fig.4. It is found that the voltage of the three phases declined from 5.8 kV to about 2.0 kV, and the current is elevated from about 0 A to 228.2 A. This is a low-resistance grounding fault of three phases. We take C phase at 1493 ms as an example and construct the simplified equivalent circuit model in Fig.5(a). Where L_C is the equivalent inductance winding of C phase transformer, H; U_C is the effective value of C phase voltage, kV; u_C is the effective voltage value of C phase transformer winding, kV; and I_C is the effective value of C phase grounding current, A. The known values for calculation are as follows: U_C=5.8 kV, u_C=2.0 kV, I_C=228.2 A. In the light of recording data, it is found that the current frequency f_1 of the low resistance grounding is 50 Hz. It can be calculated that:

$$L_C = \frac{u_C}{2\pi f_1} = 2.8 \times 10^{-2}\ \text{H} \tag{1}$$

$$r_{\text{Cu}}^C = \frac{U_C - u_C}{I_C} - R_{\text{G1}} = 0.5\ \Omega \tag{2}$$

At this stage, it is concluded that there is a three-phase line-to-ground fault, which has a great impact on the copper mesh and copper braided strip and eventually results in ground failure of the cable joints. The circuit topology diagram of the cable joints at Stage 4 is shown in Fig.5(b).

3.2. Quantitative analysis at Stage 1

The fault recording data at Stage 1 is exhibited in Fig.6. Combined with the discovery in Fig.2, it is shown that there is long-term creepage discharge at the XLPE-SiR insulation interface of C phase cable joint. It is regarded as a high-resistance grounding fault of C phase. From the current recording data, inherent small currents are existing in three phases. When the high resistance grounding fault occurs, the pulsating current appears in C phase, and its value increases from 4.2 A to more than 10 A. Simultaneously, the voltage is distorted, and the absolute peak values range from 3.4 to 5.5 kV. This situation is also responsible for the elevation in the voltage of A and B phases, which increased by 41.4% and 58.6%. We take C phase at 105 ms as an example and construct the simplified equivalent circuit model at the moment of the creepage discharge in Fig.7(a). Where R_I^C is the equivalent resistance of XLPE-SiR insulation interface of C phase joint, Ω; R_S^C is the equivalent resistance of the axial semiconducting layer, Ω; u'_C is the distorted voltage value of C phase transformer winding, kV; I'_C is the effective value of phase C pulsating grounding current, A; f_2 is the frequency of the pulsating current, Hz. The known values for calculation are as follows: u'_C =3.4 kV, I'_C =7.2 A.

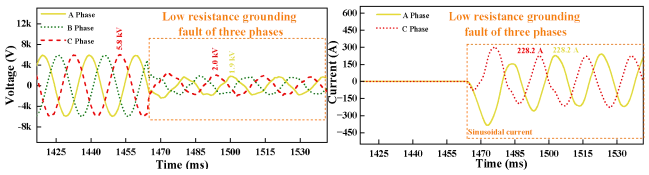

Fig.4 *The voltage and current recording data at Stage 4*

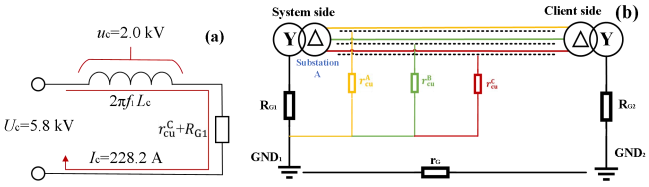

Fig.5 *Equivalent electrical models at Stage 4*
(a) Simplified equivalent circuit model of C phase, ***(b)*** Circuit topology diagram

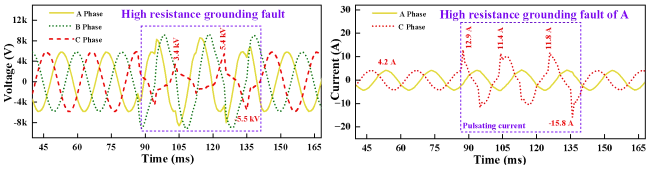

Fig.6 *The voltage and current recording data at Stage 1*

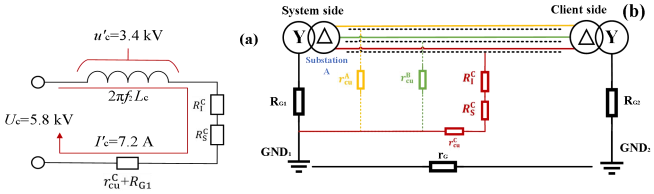

Fig.7 *Equivalent electrical models at Stage 1*
(a) Simplified equivalent circuit model of C phase at the moment of the creepage discharge, ***(b)*** Circuit topology diagram

At the time of the creepage discharge, it can be calculated that:

$$R_I^C + R_S^C = \frac{U_C - u'_C}{I'_C} - \left(R_{\text{G1}} + r_{\text{Cu}}^C\right) = 333.3\ \Omega \tag{3}$$

$$f_2 = \frac{u'_C}{2\pi L_C} = 2682.9\ \text{Hz} \tag{4}$$

It is found that the creepage discharge at the XLPE-SiR insulation interface is characterized by high frequency and large current, which is completely distinguished from partial discharge. The circuit topology diagram of the cable joints at Stage 1 is shown in Fig.7(b).

3.3. Quantitative analysis at Stage 2 and Stage 3

The fault recording data at Stage 2 is exhibited in Fig.8. It is observed that the voltage of A and B phases is lifted due to the creepage discharge of C phase. The low resistance grounding fault occurs first in phase C around 730 ms, accompanied by the voltage distortion of B phase. Eventually, the low resistance grounding fault occurs in phase B around 790 ms. We take C phase at 823 ms as an example and construct the simplified equivalent circuit model in Fig.9(a). It is observed that the grounding current is 183.0 A, which is lower than that at stage 4. This phenomenon is probably ascribed to the initial formation of

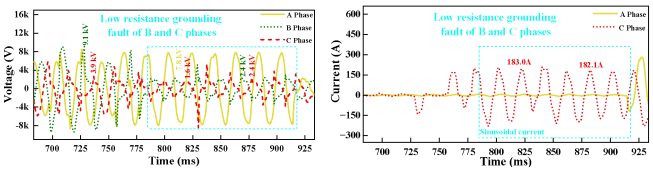

Fig.8 *The voltage and current recording data at Stage 2*

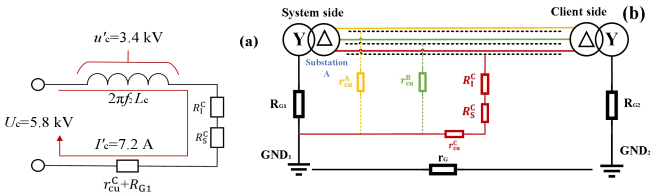

Fig.9 *Equivalent electrical models at Stage 2*
(a) Simplified equivalent circuit model of C phase, ***(b)*** Circuit topology diagram

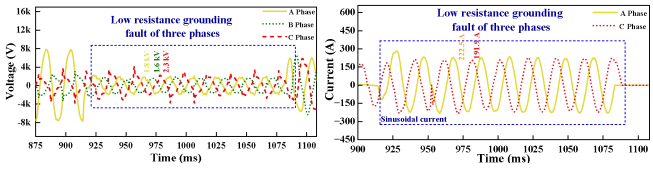

Fig.10 *The voltage and current recording data at Stage 3*

the radial breakdown channel of the SiR insulation with a certain resistance $R_{\mathrm{SiR}}^{\mathrm{C}}$. It can be calculated that:

$$R_{\mathrm{SiR}}^{\mathrm{C}} = \frac{U_{\mathrm{C}} - u_{\mathrm{C}}''}{I_{\mathrm{C}}''} - \left(R_{\mathrm{G1}} + r_{\mathrm{Cu}}^{\mathrm{C}}\right) = 7.0\ \Omega \qquad (5)$$

Thus, it is assumed that $R_{\mathrm{SiR}}^{\mathrm{C}}$ confines the carrier transport. Especially, there is still a creepage discharge feature in C phase at this stage. Therefore, the circuit topology diagram of the cable joints at Stage 2 is shown in Fig.9(b).

The fault recording data at Stage 3 is exhibited in Fig.10. Owing to the elevation in the voltage, the low resistance grounding fault occurs in A phase around 916 ms. So far, the low-resistance grounding fault has occurred to the three-phase transmission line. Contrasted with the fault recording data of Stage 4, there is still creepage discharge in phase C.

4. Validation of experiment

In order to reproduce the evolution of long-term creepage discharge at the cable joint interface of the cable joint, an operation-simulated test was conducted to analyze the behavior of the creepage discharge in the cable joint. On the one hand, this experiment is used to verify the high resistance grounding fault in Section 3 is caused by the creepage discharge; On the other hand, this experiment explains the correlation between the behavior of the creepage discharge and the carbonization degree of the XLPE insulation and the semi-conducting layer.

4.1. Preparation of cable joint samples

Three cable joints were selected from the actual 10-kV operating line in the same district. The configuration of these samples is consistent with those of the faulty cable joints. For the convenience of naming the samples, Sample

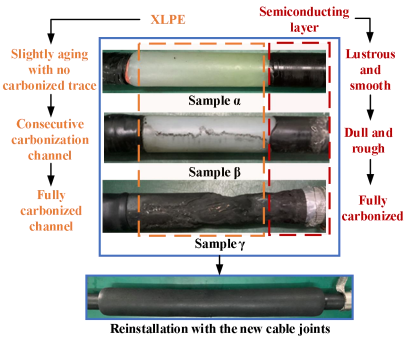

Fig.11 *Cable joint samples with different states*

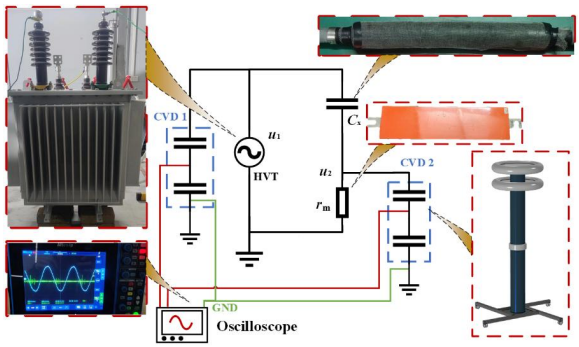

Fig.12 *The schematic diagram of the experiment*

α, β, and γ are named according to the states of the XLPE insulation and the semiconducting layer, as shown in Fig. 11. These different states of the cable samples represent the evolution of the long-term creepage discharge at the XLPE-SiR insulation interface of the cable joint. Finally, the cable samples are reinstalled with the new cable joints for the following test.

4.2. Test method

The creepage discharge voltage and current waves of the samples were measured under the high voltage condition. The purpose of the test is to explore the changes in the creepage discharge behavior of the samples with the evolution of carbonation damage. The site diagram and schematic diagram of the test are shown in Fig.12. Where HVT is the high-voltage transformer with a capacity of 110 kVA (22 kV, 5 A); r_{m} is the non-inductive resistance (20 Ω), which is applied to calculate the loop current; C_{x} is the selected sample where the conductor is connected to the high voltage, and the outer semi-conducting layer is wrapped with copper mesh and connected to r_{m}; CVD1 and CVD2 are the capacitive voltage dividers, which are applied to measure the voltages of HVT (u_1) and r_{m} (u_2). The sampling frequency of the oscilloscope is set to 1 GS/s (the sampling time, T_{s} = 1 ns) with 100 MHz bandwidth.

4.3. Experimental results

4.3.1 Experimental results of Sample α

Fig.13 exhibits the measured voltage and current waves of Sample α. There are obvious pulse currents occasionally under the high voltage of 12.6 kV. Since the SiR insulation of Sample α has no breakdown trace, it is judged that the currents are from the creepage discharge of

the XLPE-SiR insulation interface. It is found that the discharge current duration is 1.2 μs, and the amplitude is 30.5 A. When the large pulse current occurs, the voltage waveform at the power supply side is slightly distorted, and the voltage rises from 11.9 kV to 12.8 kV. It can be calculated that:

$$R_{eq}^{\alpha} = R_{I}^{\alpha} + R_{S}^{\alpha} = \frac{u_{eq}^{\alpha}}{i_{max}^{\alpha}} \quad (6)$$

Where R_{eq}^{α} is the equivalent resistance of Sample α during creepage discharge, Ω; R_{I}^{α} is the equivalent resistance of XLPE-SiR insulation interface of Sample α, Ω; R_{S}^{α} is the equivalent resistance of the axial semiconducting layer of Sample α, Ω; u_{eq}^{α} is the applied voltage of Sample α, kV; i_{max}^{α} is the amplitude of the pulse current of Sample α, A. The known values for calculation are as follows: u_{eq}^{α}=12.8 kV, i_{max}^{α}=30.5A, r_m=20.0 Ω.

It is calculated that R_{eq}^{α} is 399.7 Ω, which is lower than the equivalent resistance of C phase faulty cable joint, as shown in formula (3). Even though the applied voltages are different, it is confirmed that there has been certain carbonation damage in the faulty cable joint at the latency stage.

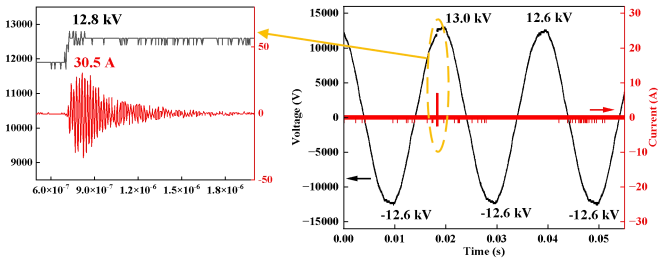

Fig.13 *The measured voltage and current waves of Sample α*

4.3.2 Experimental results of Sample β

Fig.14 exhibits the measured voltage and current waves of Sample β under the voltage of 12.6 kV. Compared with Sample α, the amplitude and frequency of the creepage discharge is much higher. The highest amplitude of the current is up to -90.5 A. Similarly, when a large pulse current occurs, the voltage waveform at the power supply side is slightly increased. It can be calculated that:

$$R_{eq}^{\beta} = R_{I}^{\beta} + R_{S}^{\beta} = \frac{u_{eq}^{\beta}}{i_{max}^{\beta}} \quad (7)$$

Where R_{eq}^{β} is the equivalent resistance of Sample β during creepage discharge, Ω; R_{I}^{β} is the equivalent resistance of XLPE-SiR insulation interface of Sample β, Ω; R_{S}^{β} is the equivalent resistance of the axial semiconducting layer of Sample β, Ω; u_{eq}^{β} is the applied voltage of Sample β, kV; i_{max}^{β} is the amplitude of the pulse current of Sample β, A. The known values for calculation are as follows: u_{eq}^{β}=-13.5kV; i_{max}^{β}=-90.5A.

It is calculated that R_{eq}^{β} is 129.2 Ω, which is only 32.3% of R_{eq}^{α}. It is indicated that the formation of consecutive carbonization channels at the XLPE insulation and the exacerbation of carbonization at the semiconducting layer result in the decline of equivalent resistance during creepage discharge. In turn, the aggravation of the creepage discharge promotes further damage to the XLPE insulation and the semiconducting layer.

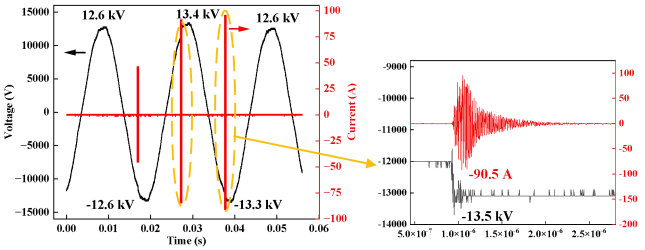

Fig.14 *The measured voltage and current waves of Sample β*

4.3.3 Experimental results of Sample γ

Fig.15 exhibits the measured voltage and current waves of Sample γ. When the original voltage is applied to 625 V, the actual voltage waveform is seriously distorted. This can be divided into two regions for analysis. Firstly, when the AC voltage rises from 0 to about 200 V, Sample γ is in the resistance-capacitance region. This means Sample γ still has the insulation characteristics. Secondly, when the voltage exceeds 200 V, there are obvious pulse currents, the maximum of which is 1.5 A. Subsequently, the generation of the currents pulls down the original voltage wave, and the sawtooth voltage waves appear. Thirdly, when the voltage rises to about 400 V, the capacitance characteristic disappears. At this time, Sample γ is in the pure resistance region and the voltage drops to 248 V. Finally, when the voltage drops to about 400 V, Sample γ re-enters the resistance-capacitance region. This phenomenon is ascribed to the capacity limitation of the high-voltage transformer. It can be calculated that:

$$R_{eq}^{\gamma} = R_{I}^{\gamma} + R_{S}^{\gamma} = \frac{u_{eq}^{\gamma}}{i_{max_m}^{\gamma}} \quad (8)$$

Where R_{eq}^{γ} is the equivalent resistance of Sample γ during creepage discharge, Ω; R_{I}^{γ} is the equivalent resistance of the XLPE-SiR insulation interface of Sample γ, Ω; R_{S}^{γ} is the equivalent resistance of the axial semiconducting layer of Sample γ, Ω; u_{eq}^{γ} is the applied voltage of Sample γ, kV; i_{max}^{γ} is the amplitude of the pulse current of Sample γ, A. The known values for calculation are as follows: u_{eq}^{γ}=72.0 V; i_{max}^{γ}=1.5 A.

It is obtained that R_{eq}^{γ} is 28.0 Ω, which is only 7.0% of R_{eq}^{α}. It is confirmed that the formation of a fully carbonized channel leads to the loss of insulation characteristics. In the actual transmission line with a large transmission capacity, huge discharge energy will be released in this insulation state, leading to a large system voltage fluctuation and a series of severe chain reactions.

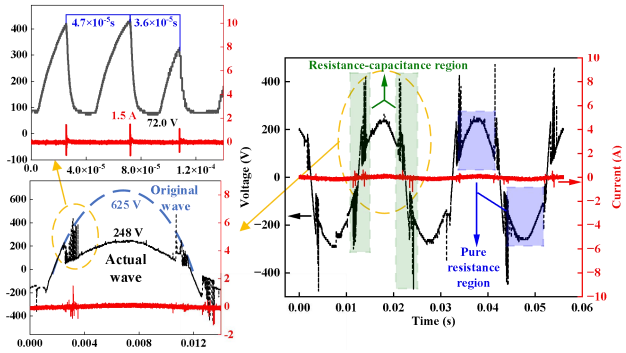

Fig.15 *The measured voltage and current waves of Sample γ*

5. Deduction of the evolution of the cable joint fault

Based on the analysis of the previous four chapters, the evolution of the cable joint fault is reorganized and divided into four stages, including latency stage, grounding failure stage, insulation failure stage, and explosion stage. The timeline of the evolution of the cable joint fault is shown in Fig.16.

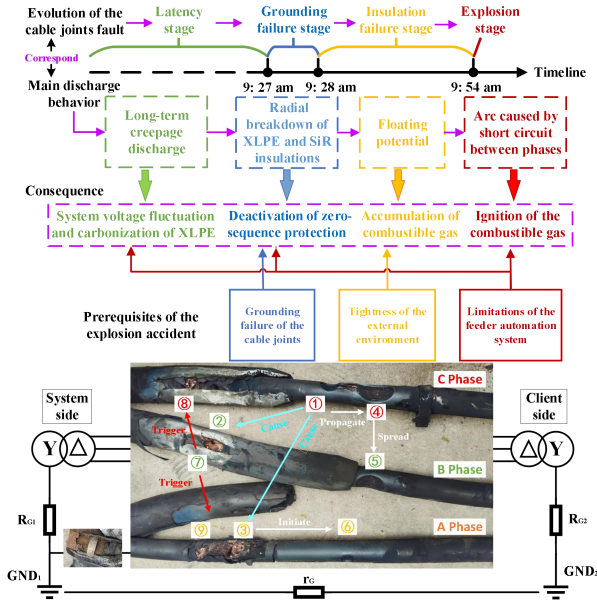

Fig.16 *The timeline of the evolution of the cable joint fault*

5.1. Latency stage

Combined Fig.16 with the fault recording data and experimental results, it is acknowledged that there is a long-term creepage discharge at the XLPE-SiR insulation interface of C phase cable joint. This process is defined as the latency stage of cable joint fault. This discharge behavior is responsible for the system voltage fluctuation and the subsequent radial insulation breakdown of the cable joints.

Creepage discharge at the XLPE-SiR insulation interface is classified as the high resistance grounding fault in the power distribution system. Due to the insensitive relay protection, the zero-sequence protection is unable to trigger. Thus, the creepage discharge at the XLPE-SiR insulation interface is the origin of the explosion accident.

5.2. Grounding failure stage

At the grounding failure stage, the grounding system of the cable joints is destructed, resulting in the deactivation of the zero-sequence protection. Combined with Fig.16, the process is illustrated as follows.

Firstly, the long-term creepage discharge is ascribed to the carbonization of the XLPE insulation. Further, the breakdown point at position ① is generated due to obvious electric field distortion. Secondly, the creepage discharge of C phase cable joint results in the elevation of the voltage of B and A phases line, inducing the breakdown points at positions ② and ③.

Eventually, 1st zero-sequence protection caused by the three-phase line-to-ground fault is activated. Subsequently, 1st reclosing operation is triggered, which has a great impact on the copper mesh and copper braided strip and eventually results in the grounding failure of the cable joints. After the subsequent 2nd zero-sequence trip protection and 2nd reclosing operation, the protection identifies the line returns to normal.

At this stage of 9:28 am, the grounding currents caused by floating potential can only flow directly to System side through the semiconducting layer of the cable joint surface, or flow back to System side through Client side with numerous resistances. This explains the carbonization of the semiconducting layer on the right side of the cables' body. Nevertheless, the grounding currents are too weak to trigger the trip protection due to the current limit of the semiconducting layer. The insulations begin to be ablated by the floating potential.

5.3. Insulation failure stage

During the period from 9:28 am to 9:54 am, the floating potential of the cable joints continuously ablates the insulations. This is a process of accumulation stage of combustible gas as well. In Fig.16, for C phase cable joint, the floating potential at position ① intensifies the axial creepage discharge and further extends to position ④ where it is the interface between the outer semiconducting layer and copper tape shield. Pyrolysis of the insulations caused by the creepage discharge produces a certain amount of combustible gas.

For B phase cable joint, the floating potential at position ② exacerbates the pyrolysis of the SiR insulation. The exposed part of the copper conductor expands, strengthening the discharge intensity. In addition, the outer semiconducting layer and the XLPE insulation are gradually carbonized and converted into combustible gas due to the high electric field at position ④.

For A phase cable joint, the floating potential at position ③ aggravates the pyrolysis of the SiR insulation and expands the area of the exposed copper conductor. The XLPE-SiR insulation interface pressure is declined due to the destruction of the cable joint. This situation may be responsible for the creepage discharge and eventually leads to the breakdown point in position ⑥. At this stage, the interior of the three-phase cable joints is full of combustible

gas. Additionally, partial combustible gas may leak into the enclosed cable trench through the broken protection shell.

5.4. Explosion stage

At 9:54 am, the explosion caused by the ignition of the combustible gas occurs. Firstly, due to the insulation failure, the interphase breakdown between position ④ and position ⑤ happens. 1st trip protection is triggered by the arc between the conductors of B and C phases. A slight explosion results in the loss of 1/2 of the whole two-phase copper conductor. In this process, the destruction of the protection shell is exacerbated. Meanwhile, a large amount of combustible gas diffuses to the enclosed cable trench, which is in full contact with the external oxygen.

At the moment of the 1st reclosing operation, the impact of the switching surge is injected into the three-phase cable joints. The exposed conductor of position ⑦ discharges to position ⑧ and position ⑨. The stable arc generated by three-phase interphase breakdown ignites the combustible gas, leading to the explosion accident.

5.5. Prerequisites of the explosion accident

From the above deduction, three prerequisites of the explosion accident can be deduced as follows.

(1) Limitations of the feeder automation system in the distribution network: the insensitive zero-sequence protection and the reclosing operation design are responsible for the destruction of the grounding system of the cable joints. Additionally, reclosing operation provides instantaneous large-capacity energy for the explosion.

(2) Grounding failure of the cable joints: this is responsible for the deactivation of zero-sequence protection. The long-term floating potential within the cable joints ablates the insulations continuously, which provides a large amount of combustible gas for the explosion.

(3) Tightness of the external environment: the enclosed cable trench accelerates the accumulation process of combustible gas, which provides a suitable site for the explosion.

6. Discussion

6.1. Initiation and development of creepage discharge at the XLPE-SiR insulation interface

Initiation of creepage discharge: From Section 2, it is discovered that there is a protrusion defect at the XLPE-outer semiconducting layer interface caused by inappropriate installation. At this position, the electric field is distorted distinctly [17, 18], and the insulation is degraded gradually. Faint partial discharge is easy to be activated and promotes the accumulation of space charges [19, 20]. After the space charges accumulate to a certain extent, intense partial discharge and surface flashover occur under the effect of humidity or other factors. A discontinuous carbonization channel begins to be generated above the XLPE insulation.

Development of creepage discharge: under the long-term partial discharge and surface flashover at the XLPE-SiR insulation interface, a consecutive carbonization channel is gradually generated as shown in Fig. 17. The more exacerbated carbonization of the channel is, the more charge carriers are allowed to transport, which in turn aggravates the carbonization of the channel. Thus, the intensity of the creepage discharge becomes increasingly strong and results in the radial insulation breakdown at position ① and position ⑥. The details will be discussed in Section 6.3.

Propagation of creepage discharge: in Fig. 2(a), it is found that there is an obvious axial insulation breakdown channel from position ① to position ④. This phenomenon is ascribed to the propagation of the creepage discharge. From the analysis of current distribution, the majority of the current is concentrated in the shadow area of the outer semiconducting layer. Under the electrical and thermal effects, axial insulation breakdown happens first in this area with high current density.

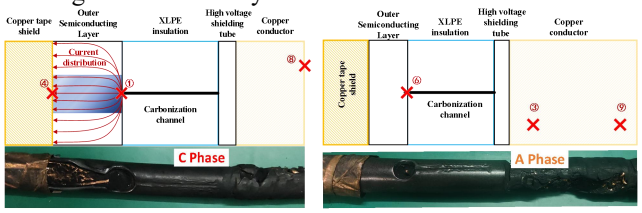

Fig.17 *Diagram of damage location of C and A phase cable joints*

6.2. Radial breakdown process of insulation

The radial breakdown point of the XLPE insulation at position ⑤ of phase B is discussed, as shown in Fig.18. In the light of the analysis of Section 5, the result shows that the XLPE insulation is ablated caused by the floating potential at position ④. The generated current gradually carbonizes the outer semiconducting layer. As the carbonization exacerbates, the electric field of the XLPE insulation becomes more distorted. The dynamic changes of the radial electric field of the XLPE insulation can be analyzed by calculating the electric field nonuniformity coefficient *f*. The calculation model is shown in Fig.19, and the calculated equations are expressed as follows [21].

$$E_{\max} = U/L_0\,\varepsilon_{\mathrm{ri}}\left(\frac{1}{\varepsilon_{\mathrm{r1}}}\ln\frac{L_1}{L_0}+\frac{1}{\varepsilon_{\mathrm{r2}}}\ln\frac{L_2}{L_1}\right) \tag{9}$$

$$E_{\mathrm{av}} = \frac{U}{L_2-L_0} \tag{10}$$

$$f = \frac{E_{\max}}{E_{\mathrm{av}}} \tag{11}$$

Where $E_{\max}$ is the maximum electric field strength in the cable insulation, kV/mm; $\varepsilon_{\mathrm{r1}}$ is the relative permittivity of the XLPE insulating layer; $\varepsilon_{\mathrm{r2}}$ is the relative permittivity of the XLPE carbonized layer; U is the voltage of the cable conductor, kV; L_0 is the radius of the cable conductor, mm; L_1 is the radius of the insulating layer, mm; L_2 is the radius of the carbonized layer, mm; E_{av} is the averaged electric field strength in the cable insulation, kV/mm. The known values for calculation are as follows: $\varepsilon_{\mathrm{r1}}$=2.3, $\varepsilon_{\mathrm{r2}}$=8.0, U=5.8 kV, L_0=11.4 mm, L_2=16.0 mm. Based on (9)-(11), it is

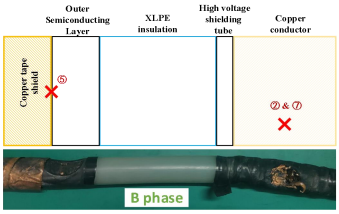

Fig.18 *Diagram of damage location of B phase cable joint*

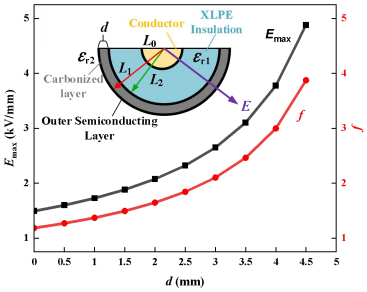

Fig.19 *Calculated model and the result of the radial breakdown process of XLPE insulation*

calculated that the correlation among carbonation depth d (L_2-L_1), E_{max}, and f, as shown in Fig.19.

In Fig.19, it is observed that E_{max} of the XLPE insulation increases abruptly with the deepening of d. When d reaches 3 mm, f>2 and it is considered as the non-uniform electric field. During this carbonized process, E_{max} becomes increasingly intensified. When carbonization reaches a certain degree, radial breakdown of XLPE insulation occurs at position ⑤.

Subsequently, the radial breakdown of the SiR insulation occurs along the breakdown channel of XLPE insulation. Eventually, the arc between the conductors of B and C phases is formed, resulting in a slight explosion. At this moment, the three-phase cable joints are full of a large amount of metallic vapor and organic gas, which provides the charged particles for the subsequent explosion.

6.3. Explosive energy and its conversion

Based on the field investigation and the disassembly analysis, the explosive energy and its conversion are calculated in this section. To simplify the explosion accident, three assumptions are established as follows. First, the insulation mass loss caused by pyrolysis is completely converted to methane (CH_4); Second, the generated CH_4 is completely combusted during the explosion; Third, CH_4 is evenly distributed in the enclosed cable trench.

According to the loss of insulation volume and the density of XLPE and SiR, the insulation mass loss of the three-phase cable joints is calculated. Subsequently, the energy released by the complete combustion of CH4, kinetic energy loss of the cement panels lifting, and air heating converted by explosive energy can be calculated by Formula (12)~(14) [22].

$$Q_{CH_4} = m_{CH_4} \cdot q_{CH_4} \tag{12}$$

$$W = Mg(h_1 + 2h_2) \tag{13}$$

$$Q_{air} = Q_{CH_4} - W = c_{air} \cdot m_{air} \cdot \Delta T \tag{14}$$

Where Q_{CH_4} is the energy generated by the complete combustion of CH_4, J; q_{CH_4} is the calorific value of CH_4, J/kg; W is kinetic energy loss of the cement panels lifting, J; M is the mass of the cement panel, kg; g is gravitational constant, N/kg; h_1 is the lifting high of one cement panel, m; h_2 is the lifting high of the other two cement panels, m; Q_{air} is the energy converted into temperature rise of air, J; c_{air} is the specific heat capacity of air at 27 ℃, J/(kg·℃); m_{air} is the mass of air in the enclosed cable trench, kg. ΔT is the temperature difference before and after the explosion, ℃. The known values for calculation are as follows: $m_{CH_4} = 44.3$ g, $q_{CH_4} = 5.6 \times 10^7$ J/kg, $M = 28.0$ kg, $g = 10.0$ N/kg, $h_1 = 3.0$ m, $h_2 = 1.0$ m, $c_{air} = 1005.0$ J/(kg·℃), $m_{air} = 9.9$ kg.

After the calculation, it is obtained that $Q_{CH_4} = 2479120.0$ J, $W = 1680.0$ J, $Q_{air} = 2477440.0$ J, $\Delta T = 248.8$ ℃. It is found that the average temperature of the whole cable trench increased to 248.8 ℃ caused by the explosion. Further, the temperature rise near the explosion point is more accentuated. It can explain the blackened cable trench and the burned-out three-phase cable joints.

7. Conclusion

The evolution of the cable joints fault companied with various discharge behaviors determines the direction of the explosion accident in the distribution network. To begin with, the long-term creepage discharge at the XLPE-SiR insulation interface is the origin of the explosion accident. This discharge behavior is characterized by large current (more than 7 A) and high frequency (more than 2500Hz), which is completely distinguished from partial discharge. Subsequently, the radial breakdown of the XLPE and the SiR insulations is generally triggered by the creepage discharge. Due to the reclosing operation of relay protection, the impact of multiple grounding currents (more than 190 A with 50 Hz) is responsible for the grounding failure of the cable joints. Further, the XLPE and the SiR insulations are ablated by the floating potential, and a large amount of combustible gas is generated in an enclosed cable trench. Eventually, due to the insulation failure, the arc discharge formed between three-phase conductors sparks the explosion by igniting the combustible gas.

Limitations of the feeder automation system in the distribution network, grounding failure of the cable joints, and tightness of the external environment are the prerequisites for this explosion accident. In the actual operation and maintenance of the power distribution system, one of the prerequisites can be eliminated to prevent this accident. On the premise of not changing the existing distribution network operation mode, online monitoring of the creepage discharge is an optimal measure to predict analogous accidents currently.

8. Acknowledgment

This research is greatly supported by the Project of Guangdong key laboratory of Clean energy technology (No. 2008A060301002), and the authors gratefully acknowledge the Shenzhen Power Supply Bureau.

9. References

[1] Torres, B., et al.: 'Integrating Smart Grid Devices into the Traditional Protection of Distribution Networks', Energies., 2022, 15,(7), pp. 2518

[2] Bonfiglio, M., Brignone, F., Delfino., R. Procopio.: 'Optimal Control and Operation of Grid-Connected Photovoltaic Production Units for Voltage Support in Medium-Voltage Networks', IEEE Transactions on Sustainable Energy., 2014, 5, (1), pp. 254-263

[3] Siebert, L., et al.: 'An Agent-Based Approach for the Planning of Distribution Grids as a Socio-Technical System', Energies., 2020, 13, pp. 4837

[4] Barreto, N., et al.: 'Artificial Neural Network Approach for Fault Detection and Identification in Power Systems with Wide Area Measurement Systems', J. Control Autom. Electr. Syst., 2021, 32, pp. 1617–1626

[5] Shirkovets, A.: 'Integral arc models at single phase-to-ground faults and special characteristics of arcing in power cable insulation', Proc. Int. Conf. Electric Power Quality and Supply Reliability, Tartu, Estonia, 2012, pp. 1-7

[6] Shirkovets, A, Telegin, A.: 'Statistical characteristics for parameters of transient processes at arcing ground faults in cable networks', Proc. Int. Conf. 2nd International Conference on Electric Power Equipment - Switching Technology (ICEPE-ST), Matsue, Japan, 2013, pp. 1-4

[7] Bernards, R., Morren, J., Slootweg, H.: ' Impact of arc impedance on earth fault currents in medium voltage cable networks', Proc. Int. Conf. 2015 IEEE Eindhoven PowerTech, Eindhoven, Netherlands, 2015, pp. 1-6

[8] Elayyan, H., Abderrazzaq, M.: 'Electric field computation in wet cable insulation using finite element approach', IEEE Transactions on Dielectrics and Electrical Insulation., 2005, 12, pp. 1125-1133

[9] Liu, X., Hou, D., Ji, J., Zhu, H.: 'Experiment and numerical simulation of cable trench fire detection', Case Studies in Thermal Engineering., 2021, 28, pp. 101338

[10] Dong, X., et al.: 'Analysis of cable failure modes and cable joint failure detection via sheath circulating current', Proc. Int. Conf. 2014 IEEE Electrical Insulation Conference (EIC), Philadelphia, PA, USA ,2014, pp. 294-298

[11] Jiang, Y., Min, H., Luo, J., et al.: 'Partial Discharge Pattern Characteristic of MV Cable Joints with Artificial Defect', Proc. Int. Conf. China International Conference on Electricity Distribution, IEEE, Nanjing, China, pp. 1–3, 2011

[12] Arief, Y., Ahmad, H., Hikita, M.: 'Partial discharge characteristics of XLPE cable joint and interfacial phenomena with artificial defects', Proc. Int. Conf. 2008 IEEE 2nd International Power and Energy Conference, Johor Bahru, Malaysia, 2008, pp. 1518-1523

[13] Li, G., et al.: 'Insulation Properties and Interface Defect Simulation of Distribution Network Cable Accessories Under Moisture Condition', IEEE Transactions on Dielectrics and Electrical Insulation., 2022, 29, 2, pp. 403-411

[14] Huang, J., Ye, Z., Zhang, G., Bao, S., Wang, P., Liu, G.: 'Study on a 110 kV combined prefabricated joint fault caused by premature failure of grounding grid', Engineering Failure Analysis., 2022, 141, pp. 106701

[15] Liao, Y., Bao, S., Xie, Y., Zhao, Y., Wang, P., Liu, G., Hui, B., Xu, Y.: 'Breakdown failure analysis of 220 kV cable joint with large expanding rate under closing overvoltage', Engineering Failure Analysis., 2021, 120, pp. 105086.

[16] Hu, R., Liu, G., Huang, C., Xu, Z., Zhou, W.: 'Power cable fired by transient arcing below the action value of relay protection: An analysis of a medium-voltage cable joint breakdown fault', Engineering Failure Analysis., 2023, 145, pp. 107028.

[17] Nebojša, B., Raičević.: 'Electrical Field Modelling at the Cable Joints', Electrical Engineering., 2007, 20, (1), pp. 9-20.

[18] Li, G., et al.: 'Insulation Properties and Interface Defect Simulation of Distribution Network Cable Accessories Under Moisture Condition', IEEE Transactions on Dielectrics and Electrical Insulation., 2022 ,29(2), pp. 403-411.

[19] Ouyang, B., Li, H., Zhang, X.: 'The role of micro-structure changes on space charge distribution of XLPE during thermo-oxidative ageing', IEEE Transactions on Dielectrics and Electrical Insulation., 2017, 24, (6), pp. 3849-3859

[20] Fleming, R., Henriksen, M.: 'The influence of electrodes and conditioning on space charge accumulation in XLPE', IEEE Transactions on Dielectrics and Electrical Insulation., 2002, 7, (4), pp. 561-571

[21] Kuffel, J., Kuffel, E.: 'High Voltage Engineering Fundamentals', Science Press, Second edition, 2000.

[22] S, Yang., W, Tao.: 'Heat Transfer', Higher Education Press, Fourth edition, 2006.